Check for updates

*Progress in Photovoltaics: Research and Applications*

WILEY

PROGRESS IN PHOTOVOLTAICS

RESEARCH ARTICLE OPEN ACCESS

# $CdCl_2$ Treatment for $Cu_2ZnSn(S,Se)_4$: A Method to Enhance the Solar Cell Performance

Prabeesh Punathil[1] | Elisa Artegiani[1] | Solidea Zanetti[2] | Simya O K[1] | Luca Lozzi[3] | A. Gasparotto[4] | Fabio Piccinelli[5] | C. L. Boldrini[5] | S. Binetti[6] | Alessandro Romeo[1]

[1]LAPS-Laboratory for Photovoltaics and Solid State Physics, Department of Computer Science, University of Verona, Verona, Italy | [2]Isopan S.p.A., Trevenzuolo, Italy | [3]Department of Physical and Chemical Sciences, University of L'Aquila, L'Aquila, Italy | [4]Department of Physics and Astronomy, University of Padova, Padova, Italy | [5]Department of Biotechnology, University of Verona, and INSTM, UdR Verona, Verona, Italy | [6]University of Milano-Bicocca, Department of Material Science, Milan, Italy

**Correspondence:** Alessandro Romeo (alessandro.romeo@univr.it)

**Received:** 15 November 2024 | **Revised:** 30 May 2025 | **Accepted:** 11 November 2025

## ABSTRACT

Unlike other thin-film absorbers, CZTSSe can be efficiently produced using nonvacuum techniques, which enable precise control over the stoichiometry of the absorber layer from the precursor solution stage. Despite extensive research over the past two decades, CZTSSe has not surpassed an efficiency of 15%, primarily due to a significant $V_{oc}$ deficit. To address this challenge, researchers typically pursue either alloying the absorber with additional elements to tune the band gap or doping the absorber with impurities to boost carrier concentration. This study presents a straightforward approach for improving performance by either narrowing the band gap or doping the absorber by processing, for the first time, the CZTSSe by $CdCl_2$ treatment, which can be applied to any fabrication process. Depending on the stage of the fabrication process at which it is carried out, the same practical $CdCl_2$ treatment can introduce Cd into the CZTSSe matrix as an alloying or doping agent.

## 1 | Introduction

Thin-film solar cells are still promising for terrestrial and space photovoltaics because they allow different device designs. They use a minimal amount of material and a relatively low process temperature (compared with silicon-based photovoltaics), and they can be produced from pure glass to the final encapsulated module in the same production line. Despite having guaranteed a reduced €/Wp in some cases, especially in Europe, they could not gain significant market shares. The thin-film technology that has achieved the highest conversion efficiency is based on $Cu_2InGaSe_2$ (CIGS) absorber material, with a record efficiency of 23.6% [1]; following this technology but intending to replace rare earth elements such as In and Ga with more abundant alternatives, a family of materials, called kesterites, has been considered. Within this framework, the most studied compounds are $Cu_2ZnSnS_4$ (CZTS), $Cu_2ZnSnSe_4$ (CZTSe), and $Cu_2ZnSn(S,Se)_4$ (CZTSSe). These perform band gaps ranging from 1 to 1.5/1.6 eV while the CZTSSe band gap can be modulated by changing the S/Se ratio [2–4]. The combination of S and Se allows for tuning the band gap, which is also in the vision of tandem structures with improved structural, optical, and electrical properties [5, 6].

In contrast with other thin film absorbers, CZTS can also be successfully fabricated using nonvacuum techniques. With these, it is possible to control the stoichiometry of the absorber layer already in the precursor solution [7]. In this case, optimizing the precursor layer is very important for the influence on the absorber layer properties and, hence, the efficiency [8–11].

Despite extensive research on CZTSSe by various groups over the past 20 years, the highest efficiency obtained still does not exceed 15% [1]. This relatively lower efficiency, compared with other thin film solar cells, is mainly due to a large $V_{oc}$ deficit. To overcome this critical limitation, two different paths are generally followed [12]: (1) alloying the absorber with

This is an open access article under the terms of the Creative Commons Attribution License, which permits use, distribution and reproduction in any medium, provided the original work is properly cited.

© 2025 The Author(s). Progress in Photovoltaics: Research and Applications published by John Wiley & Sons Ltd.

additional elements to tune the band gap [13] or (2) dope the absorber by adding impurities to increase the carrier concentration [14].

Previously, we have studied the incorporation of different impurities, such as Ge, Na, and K [14], as well as Li, to increase the carrier concentration and passivate the defects [3, 15]. All these impurities were added by depositing chlorine compounds (NaCl, KCl, $GeCl_4$, LiCl), and we have registered structural changes for all the cases but with a particularly efficient doping effect for $GeCl_4$; Ge inclusion delivers crystallites and grains with larger size, a reduced Se incorporation and higher carrier concentration that results in higher efficiency. Cadmium, in this sense, can replace zinc ions in the material's structure, as they have similar ionic sizes.

It has been reported that the formation energy of $Cd_{Zn}$ is lower than that of both $Cu_{Zn}$ and $Zn_{Cu}$ in the $Cu_2Zn_{1-x}Cd_xSn(S,Se)_4$ (CZTSSe) compound [16]. As a result, Cd doping is expected to replace Zn, forming $Cd_{Zn}$ in Cd-doped CZTSSe. On one hand, $Cd_{Zn}$ can reduce the occurrence of $Cu_{Zn}$ antisite defects, which lessens the Fermi level pinning effect, allowing for larger band bending. On the other hand, it can also decrease the lattice mismatch between CZTSSe and CdS [17, 18], thereby reducing the recombination rate of photo-generated electrons and holes. These two effects contribute to an increased open-circuit voltage ($V_{oc}$) in CZTSSe solar cells, ultimately boosting their conversion efficiency as also mentioned by Grenet et al. [19].

Moreover, including the Cd element in the CZTSSe matrix has been shown to lower the band gap by reducing the conduction band level [20]. When this occurs, we believe that a correct interpretation of the data is to consider cadmium as an alloying element instead of doping. The band gap of CZTSSe already depends on the ratio of sulfur to selenium (Se lowers the band gap relative to sulfur); however, it can be influenced also by additional elements in the stoichiometry [19, 21]. Moreover, the elements can also affect the S/Se through the absorber resulting in a different band grading [21, 22]. Thus, the inclusion of an additional element, like cadmium, could affect the S/Se composition throughout the absorber, resulting in a different grading of the band gap.

In this work, we introduce a straightforward and adaptable method to enhance the device efficiency by either tuning the band gap or doping the absorber layer by the incorporation of cadmium respectively as an alloying/doping element into the CZTSSe absorber with a very simple and applicable $CdCl_2$ processing step, never introduced before for CZTSSe.

## 2 | Materials and Methods

### 2.1 | Solar Cell Fabrication

In our laboratories, the CZTSSe device is fabricated on substrate configuration, on a soda lime glass (see Figure 1) [14, 23]. A bilayer stack of molybdenum is deposited by RF sputtering from a 3-in. diameter Mo target (99.95% purity) as back contact. A first, more adhesive Mo layer, with a thickness of 700 nm, is deposited at a pressure of 1 Pa by an argon flux of 30 sccm with a sputtering power of 100 W, whereas a second, more conductive, 500-nm-thick Mo layer is deposited at a lower pressure of 0.1 Pa by an argon flux of 20 sccm and with a higher sputtering power of 150 W. Both layers are deposited at a substrate temperature of 200°C.

The precursor solution is deposited onto the Mo-coated SLG substrate by spin coating at 2400 rpm for 15 s, followed by a drying step at 300°C in an air atmosphere for 5 min. This step is repeated five times to obtain a thickness of 1.6 μm. The precursor solution is based on dissolving elements like Cu, Zn, Sn, and urea-based compounds in ethanol. Notably, we dissolve copper(II) acetate monohydrate ($C_4H_8CuO_5$, purity ≥ 99%, 0.574 M, obtainable from Merck Chemicals), zinc(II) acetate dihydrate ($C_4H_{10}O_6Zn$, purity ≥ 99%, 0.375 M, from Sigma Aldrich), tin(II) chloride dehydrate ($SnCl_2$ $2H_2O$, purity ≥ 98%, 0.3 M, from Fluke chemicals), and thiourea ($NH_2CSNH_2$, purity 99%, 2.4 M, from Sigma Aldrich) into 2-methoxy ethanol ($CH_3OCH_2CH_2OH$, purity ≥ 99.8%, from

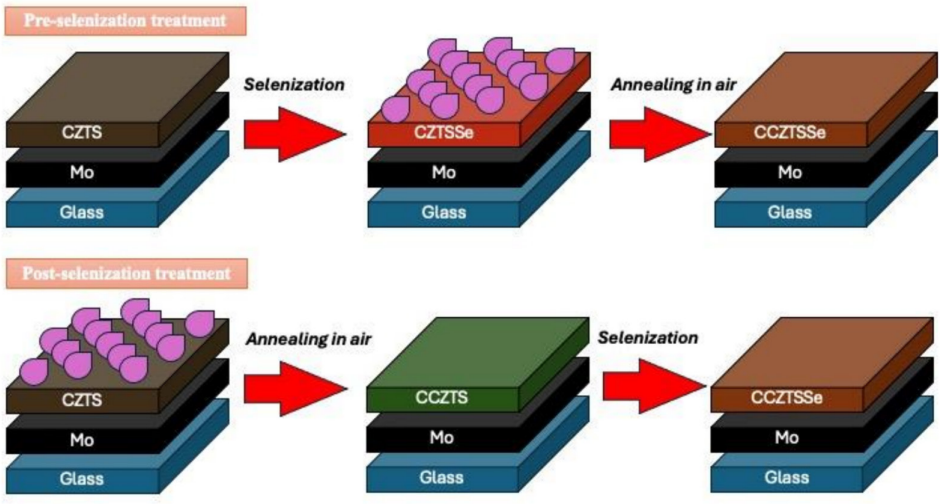


**FIGURE 1** | Scheme of the two different $CdCl_2$ treatment processes that are compared in this work.



1099159x, 0, Downloaded from https://onlinelibrary.wiley.com/doi/10.1002/pip.70034 by Universita Milano Bicocca, Wiley Online Library on [25/11/2025]. See the Terms and Conditions (https://onlinelibrary.wiley.com/terms-and-conditions) on Wiley Online Library for rules of use; OA articles are governed by the applicable Creative Commons License

Sigma Aldrich). In this respect, a stabilizer, such as diethanolamine ($HN(CH_2CH_2OH)_2$, purity ≥98%, obtainable from Sigma Aldrich), is added during the step of preparing a precursor solution.

Subsequently, a so-called "selenization" step of the CZTS precursor film is provided to transform the precursor into a crystallized stoichiometric absorber layer: the CZTS precursor film is annealed at 450°C for 30 min in a selenium atmosphere to complete the phase formation, enhance the crystalline quality, and incorporate selenium into the crystal lattice, finally obtaining the CZTSSe structure [23]. The annealing is performed in a previously evacuated tube ($10^{-4}$ Pa) together with 0.3 g of Se pellets with an Argon pressure of $2*10^{-3}$ Pa. A Nabertherm-TSH12 single-zone horizontal tube furnace is used for this selenization, and it is equipped with a turbomolecular pump and pressure monitor system. After the absorber fabrication, a 60 nm-thick CdS as a buffer layer is applied by chemical bath deposition. In particular, 15 mL of cadmium acetate dihydrate ($Cd(CH_3COO)_2\ 2H_2O$) solution (purity 98%, 0.025 M, from Merck chemicals), 10 mL of thiourea (0.422 M), and 25 mL of ammonia ($NH_4OH$, 20%) solution are added to 200 mL of distilled water. The deposition is done at 60°C for 10 min. The front contact consists of an 80-nm-thick intrinsic zinc oxide and 1-μm-thick conductive indium tin oxide (ITO) layer, deposited by RF sputtering.

The deposition is carried out with 3-in. targets and with a power of 60 W for ZnO and 160 W for ITO, respectively, at a substrate temperature of 150°C and continuous oxygen flux ($O_2$: 0.5 sccm).

Finally, a 30-nm-thick Au grid is deposited through shadow masks using the thermal evaporation technique, and the cell active area (0.13 $cm^2$) is identified by mechanical scribing. This metal contact, deposited on top of the devices, improves the collection of photo-generated carriers in the solar cell.

### 2.2 | Selenization and $CdCl_2$ Treatment of CZTSSe Films

In addition to the above-described process, we introduce here a Cd inclusion step that can be added to the process either before or after the selenization, respectively, preselenization or postselenization treatment (see Figure 1). The addition of the cadmium into the absorber layer is carried out by adding drops of $CdCl_2$ hemi(pentahydrate) ($CdCl_2{\cdot}2½H_2O$, 79.5%–81%, 40 mM, from Sigma Aldrich) dissolved in methanol.

- For the preselenization treatment (from now on identified as "BS": before selenization), the $CdCl_2$ solution is drop-cast onto the CZTS precursor films, followed by drying on a hotplate at 150°C for 3 min and rinsing with distilled water.
- For the postselenization treatment (from now on identified as "AS": after selenization), the selenized CZTSSe films are similarly drop-cast with the $CdCl_2$ solution, followed by drying on a hotplate at 150°C for 3 min and rinsing with distilled water.

### 2.3 | Characterization Techniques

The absorbers have been analyzed in terms of physical and electrical properties. Scanning electron microscopy (SEM) analysis was applied with a Zeiss Gemini500 and energy dispersive X-ray spectroscopy (EDXS) detector. Raman spectra were processed by a Horiba Jobin-Yvon LabRam HR800 microprobe setup (in backscattering geometry) by exciting radiation at 532 and 408 nm (He–Ne laser). XRD patterns were recorded by Thermo ARL X'TRA powder diffractometer in Bragg–Brentano geometry, equipped with a Cu-anode X-ray source (Kα, $\lambda = 1.5418$ Å) and Peltier Si (Li) cooled solid-state detector (Cukα X-ray irradiation with sampling width of 0.02°). The MAUD program was used to perform the Rietveld refinement on the diffraction data to determine the lattice parameters and the average crystallites' size.

Also, SIMS depth profiles have been processed to identify the diffusion of the elements through the device. They have been processed on a CAMECA IMS-4f using a $Cs^+$ primary ion beam at a 10-kV accelerating voltage (corresponding to 5.5-keV impact energy) and detection of positive secondary ions.

External Quantum Efficiency (EQE) measurements were recorded as a function of the excitation wavelength (350–1400 nm) using a monochromator (Lot-Oriel Omni-λ300) and a halogen lamp (100 W) as the incident light in AC mode. The monochromatic light was mechanically chopped at a frequency of 75 Hz, and the photocurrent response was measured using a lock-in amplifier.

Electrical properties have been performed, in particular capacitance–voltage (CV) and drive level capacitance profiling (DLCP) by an HP4284A LCR.

## 3 | Results and Discussion

### 3.1 | Change in the Performance

The typical efficiency of our standard devices, fabricated at low-temperature selenization and with a nonvacuum deposition technique for the absorber layer, falls within the range of 5%. This low selenization temperature (450°C vs. 550°C) has been carried out for flexible applications. Preliminary results show an increase of 40% in the base efficiency (more than 7%) with a 550°C selenization temperature.

However, this paper is expressly based on the comparison with and without $CdCl_2$ treatment, so the 450°C selenization process has been considered in this work, comparing the devices made with preselenization and postselenization $CdCl_2$ treatment. These treatments have been tested with different amounts of $CdCl_2$ solution, namely, 5, 10, and 15 drops, and their JV parameters are presented in Table 1, with the acronyms that will be used in this paper; also, respective JV curves are shown in Figure 2.

The initial efficiency of the reference sample (not treated) increases substantially with the treatment. In particular, the



1099159x, 0, Downloaded from https://onlinelibrary.wiley.com/doi/10.1002/pip.70034 by Universita Milano Bicocca, Wiley Online Library on [25/11/2025]. See the Terms and Conditions (https://onlinelibrary.wiley.com/terms-and-conditions) on Wiley Online Library for rules of use; OA articles are governed by the applicable Creative Commons License

**TABLE 1** | Best JV parameters of CZTSSe solar cells made with different $CdCl_2$ treatments.

| Treatment | $V_{oc}$ (mV) | $J_{sc}$ (mA/cm$^2$) | *FF* (%) | $\eta$ (%) |
|---|---|---|---|---|
| No treatment (reference) | 334 | 28 | 58 | 5.4 |
| 5 drops $CdCl_2$ before selenization (BS05) | 318 | 38 | 53 | 6.4 |
| 10 drops $CdCl_2$ before selenization (BS10) | 332 | 35 | 56 | 6.5 |
| 15 drops $CdCl_2$ before selenization (BS15) | 325 | 32 | 54 | 5.6 |
| 5 drops $CdCl_2$ after selenization (AS05) | 360 | 34 | 58 | 7.1 |
| 10 drops $CdCl_2$ after selenization (AS10) | 349 | 41 | 59 | 8.5 |
| 15 drops $CdCl_2$ after selenization (AS15) | 325 | 36 | 56 | 6.5 |

*Note:* In red is the highest efficiency achieved.

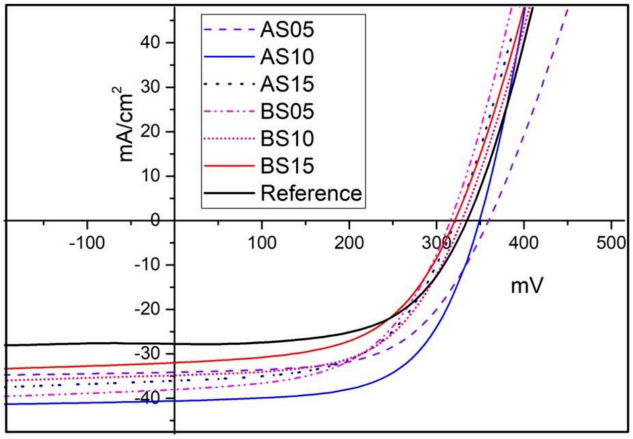


**FIGURE 2** | *J–V* curves of best devices fabricated with different $CdCl_2$ treatment and compared with the reference case (no treatment).

open circuit voltage values are higher than 10% of the not-treated sample, with the highest value being 360 mV in the case of five drops after selenization (very near to the value performed from AS10). On the other hand, the $V_{oc}$ does not substantially change for the case of $CdCl_2$ treatment before selenization. The current density increases for all treated cases, with high values for 10 drops after selenization and for 5 drops before selenization, respectively 41 and 38 mA/cm$^2$. The fill factor does not seem to be particularly affected by the treatment; only a slight reduction is observed for the samples treated before selenization.

The statistical data presented in Figure 3 also confirm these results. The efficiencies are again consistently higher for the AS10 case and generally higher for the treatment after selenization, particularly with higher $J_{sc}$ values.

In summary, $CdCl_2$ provides an increase in performance: a large increase in current density for the absorbers treated after the selenization and a smaller increase for the ones treated before the selenization. This last case also shows a general slight reduction of the $V_{oc}$, while for the first case, the $V_{oc}$ also increases.

This suggests that there are different effects of the $CdCl_2$ treatment before and after selenization, which need to be addressed.

However, it is noteworthy that simply adding a few drops of $CdCl_2$ solution during the standard CZTSSe fabrication process results in an increase in efficiency of more than 50%, thus from 5.4% to 8.5%.

A comparison of JV in the dark for the AS, BS, and reference cases has been processed; to calculate the diode ideality factor ($n$) and the reverse saturation current ($J_0$) for the CZTSSe solar cell, we use the dark current–voltage characteristics in the semi-logarithmic scale (see Figure 4).

$$J = J_0\left(e^{\frac{qV}{nkT}} - 1\right)$$

The extracted ideality factor of 1.8 for not-treated CZTSSe drops respectively to 1.65 and to 1.6 for AS and BS cases. Reverse saturation current ($J_0$) is very similar for reference ($1.06\times10^{-5}$ A/cm$^2$) and AS10 ($3.37\times10^{-5}$ A/cm$^2$), while is one order of magnitude below for BS ($5.56\times10^{-6}$ A/cm$^2$). Finally, despite shunt resistance is in the same order of magnitude for all the three cases (respectively 1488, 870, and 1358 Ω cm$^2$), the series resistance drops to half for the BS case (respectively 1.71, 1.66, and 0.81 Ω cm$^2$). This again suggests that there is a large absorber transformation for the BS case, but a device improvement is also observed for the AS case. For this reason, we have analyzed the different cases in terms of structural and electronic parameters.

## 3.2 | Structural Changes

### 3.2.1 | SEM and EDXS Analysis

Typically, $CdCl_2$ is known for its application on CdTe-based devices. In this case, a layer of $CdCl_2$ is deposited on the absorber either by vacuum evaporation or by wet deposition followed by annealing in air at a temperature in the range of 380°C–450°C [24]. In that case, a recrystallization effect is registered, which strongly affects the grains' morphology with a typical enlargement of the grain size up to 5 times for low substrate temperature deposited CdTe (i.e., vacuum evaporation).



1099159x, 0, Downloaded from https://onlinelibrary.wiley.com/doi/10.1002/pip.70034 by Universita Milano Bicocca, Wiley Online Library on [25/11/2025]. See the Terms and Conditions (https://onlinelibrary.wiley.com/terms-and-conditions) on Wiley Online Library for rules of use; OA articles are governed by the applicable Creative Commons License

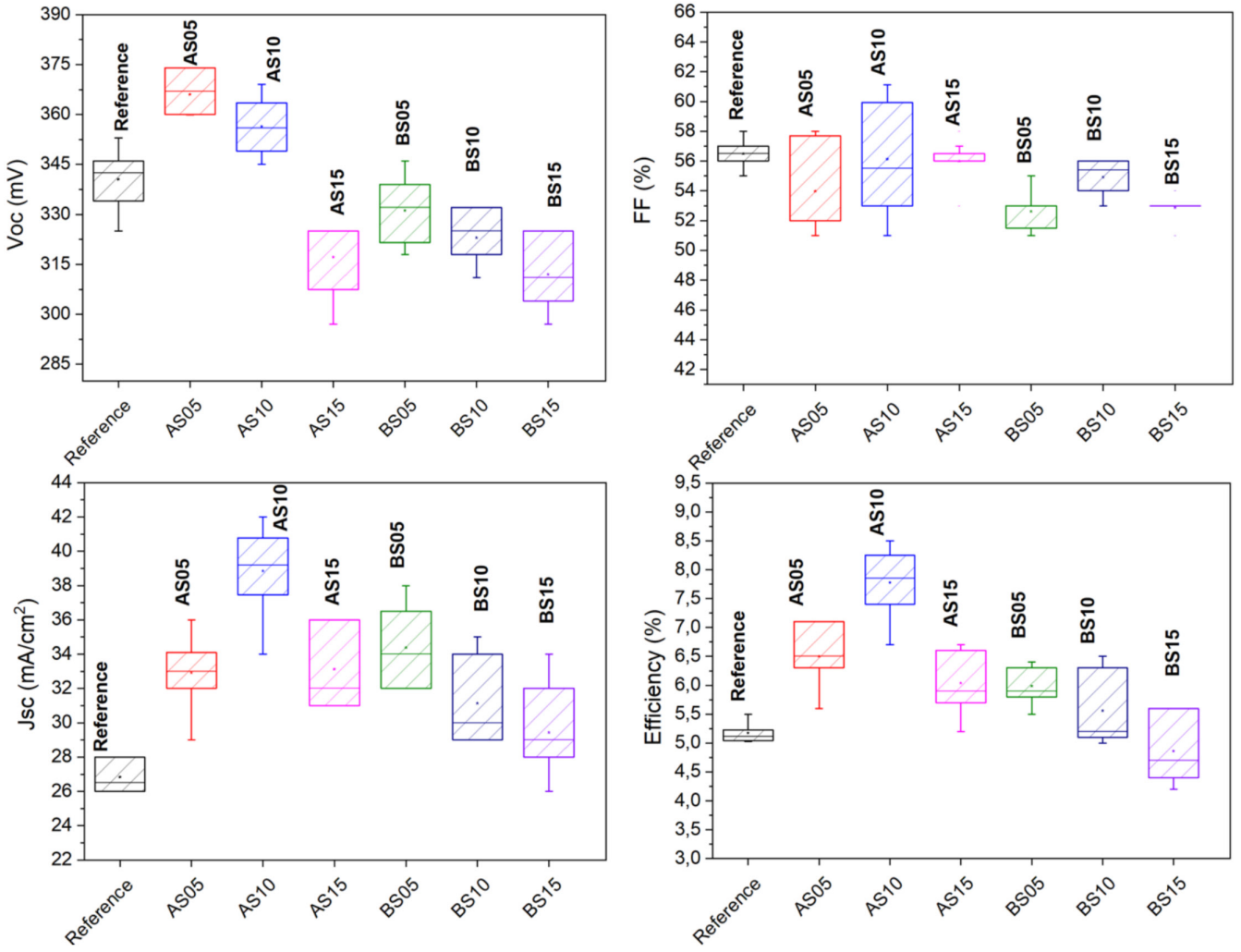


**FIGURE 3** | Statistical data (median [line], average [dot], standard deviation, and maximum and minimum values) on the performance parameters of the devices with different $CdCl_2$ treatments.

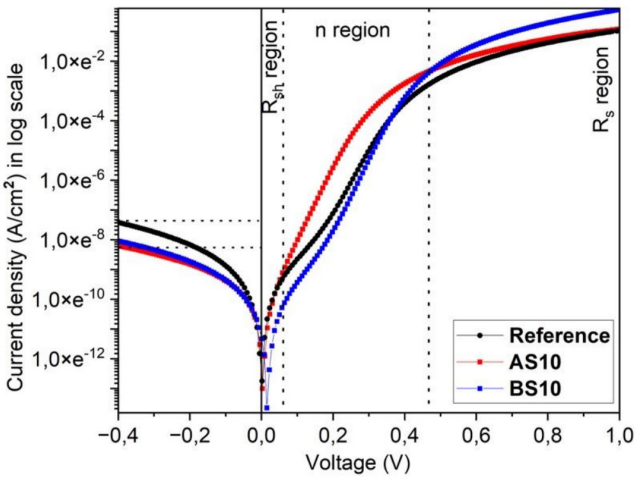


**FIGURE 4** | Logarithmic plot of JV in the dark at room temperature of CZTSSe, without treatment, treated before selenization, and treated after selenization.

The explanation of this phenomenon for CdTe layers was given by McCandless et al.: Te is brought to the gas phase according to the following chemical reaction: $CdCl_2$ (s) + $O_2$ (g) + CdTe (s) ⇌ $TeCl_2$ (g) + 2CdO (s) [25].

For CZTSSe, the $CdCl_2$ treatment does not significantly change the morphology, as it is possible to observe from the SEM analysis shown in Figure 5, where three cases are compared (reference, BS10, and AS10).

There is a slight change in the morphology with a tendential increase in the average grain size when treated before selenization. However, no significant change is observed when the treatment is done after selenization, though its effect is minimal. This suggests that the chemical dynamics for $CdCl_2$ and CZTSSe are substantially different from those described above for CdTe.

Instead, if we analyze the samples by EDXS, studying different areas for each sample, we can observe some significant



1099159x, 0, Downloaded from https://onlinelibrary.wiley.com/doi/10.1002/pip.70034 by Universita Milano Bicocca, Wiley Online Library on [25/11/2025]. See the Terms and Conditions (https://onlinelibrary.wiley.com/terms-and-conditions) on Wiley Online Library for rules of use; OA articles are governed by the applicable Creative Commons License

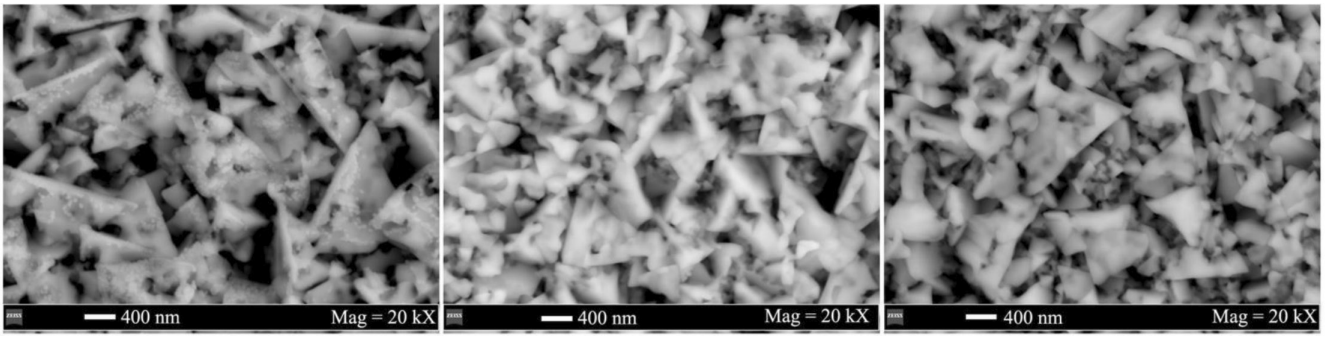


**FIGURE 5** | CZTSSe morphology: left, not-treated sample; center, treated before selenization; right, treated after selenization.

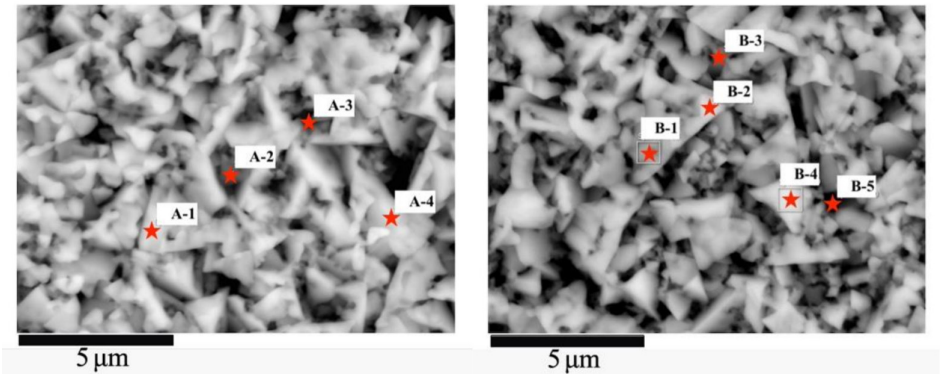


**FIGURE 6** | EDX areas (bulk and grain boundaries) taken on $CdCl_2$ treated before selenization (left); and on $CdCl_2$ treated after selenization (right).

**TABLE 2** | Comparison of the EDXS results for the composition of the absorber when treated before or after selenization at different spots (see Figure 6).

| | Treatment before selenization (BS) | | | | Treatment after selenization (AS) | | | | |
|---|---|---|---|---|---|---|---|---|---|
| **wt%** | **A1** | **A2** | **A3** | **A4** | **B1** | **B2** | **B3** | **B4** | **B5** |
| Se | 38.3 | 37.6 | 37.4 | 37.5 | 39.2 | 37.4 | 40.0 | 39.2 | 37.8 |
| Sn | 21.1 | 21.2 | 22.9 | 17.9 | 18.8 | 15.9 | 19.3 | 16.6 | 24.4 |
| Cu | 17.5 | 20.1 | 19.8 | 21.3 | 20.3 | 20.6 | 20.0 | 20.5 | 18.6 |
| Zn | 9.7 | 9.2 | 8.8 | 9.6 | 10.8 | 11.4 | 10.8 | 11 | 9.4 |
| C | 8.6 | 6.5 | 6.1 | 8.8 | 8.2 | 11.1 | 7.2 | 10.4 | 5.5 |
| S | 3.0 | 4.0 | 4.1 | 3.2 | 2.8 | 2.5 | 2.6 | 2.3 | 3.5 |
| Cd | **0.7** | **0.7** | **0.6** | **0.7** | — | — | — | — | **0.7** |
| O | 1.0 | 0.7 | — | 0.9 | — | 1 | — | — | — |
| Cl | — | 0.2 | 0.2 | 0.1 | — | — | — | — | 0.2 |

*Note:* Cd presence is highlighted in blue.

differences when we compare the three cases. Here, we compare the treatment cases before and after selenization (BS10 and AS10), and we have collected X-ray energies from the grains and grain boundaries (see Figure 6).

If the $CdCl_2$ treatment is processed before selenization, cadmium is detected in the grains (A-1 and A-4) (see Table 2), suggesting that it has been incorporated into the kesterite matrix. In contrast, if the $CdCl_2$ treatment is processed just after the selenization, no cadmium is detected in the grains, but it is present at the grain boundaries (B5). Although the variation in grain size after Cd introduction is minimal compared with other cases in the literature [17] [26], we have the confirmation that cadmium has been incorporated in the CZTSSe matrix, but only when treatment is performed before the selenization. This could be coherent with the fact that selenization is the processing step that allows the formation of the absorber. Therefore only in the BS cases does cadmium react with other elements and bond in the crystal lattice.



1099159x, 0, Downloaded from https://onlinelibrary.wiley.com/doi/10.1002/pip.70034 by Universita Milano Bicocca, Wiley Online Library on [25/11/2025]. See the Terms and Conditions (https://onlinelibrary.wiley.com/terms-and-conditions) on Wiley Online Library for rules of use; OA articles are governed by the applicable Creative Commons License

However, it is essential to highlight that cadmium is present at the grain boundaries for the $CdCl_2$ treatment processed after selenization, and this may be connected to the higher efficiency recorded for this case.

So, the morphology is not particularly affected, but cadmium is present in the structure of the absorber contributing to the improved performance; how is this happening? To further analyze the structure and understand the incorporation of cadmium, XRD and Raman have been processed for BS05, BS10, BS15, AS05, AS10, and AS15 cases.

### 3.2.2 | XRD Analysis

From the XRD patterns, shown in Figure 7, the primary CZTSSe reflections are present for all the samples, with no differences in the orientation of the peaks. On average, the crystallite size of BS samples is smaller than that of AS samples, as calculated by Rietveld refinement on the collected powder patterns (calculated 70 nm, on average vs. 100 nm for AS samples; Table 3). This finding suggests the influence of the Cd ions on the crystals' growth, which seems to be smaller when $CdCl_2$ treatment is performed before selenization (in accordance with the SEM results) and the transition metal ion is included in the matrix. The repetition of the same reflections for all the different cases, with similar relative intensities, states that no recrystallization and no reorientation of the grains occur as a consequence of the treatment with Cd ions.

The structural parameters used for XRD refinement are taken from the literature [189282-ICSD card number]. The best structural model for the refinement is the tetragonal kesterite-type crystal structure [space group: *I-4* (no. 82)]. The cubic Mo crystal structure (space group: *Fm3m* [no. 225]) has also been considered during the refinement. Refined lattice parameters are given in Table 3.

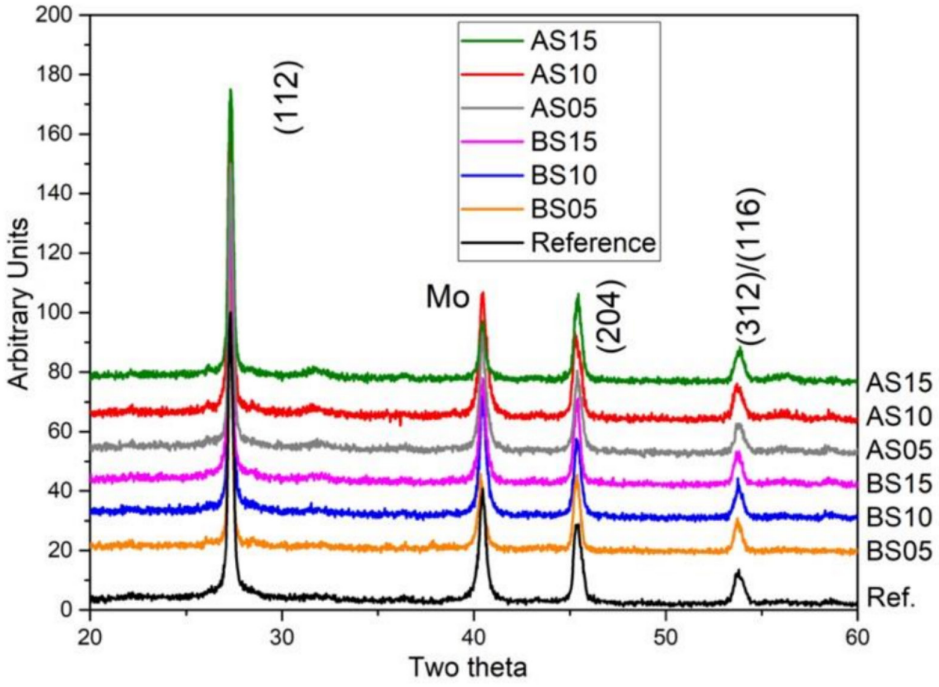


**FIGURE 7** | XRD patterns of the CZTSSe: reference (not treated absorber) compared with treated absorbers (with 5, 10, and 15 drops—05, 10, 15) before (BS) and after (AS) selenization.

**TABLE 3** | Refined lattice parameters and crystallite sizes of CZTSSe films with different $CdCl_2$ treatments.

| Sample | $a = b$ (Å) | $C$ (Å) | $V$ (Å$^3$) | Crystallite size (nm) |
|---|---|---|---|---|
| BS05 | 5.673(1) | 11.232(3) | 361.5(1) | 71(1) |
| BS10 | 5.651(1) | 11.307(3) | 361.1(1) | 72(1) |
| BS15 | 5.656(1) | 11.312(1) | 361.9(1) | 71(1) |
| AS05 | 5.648(1) | 11.293(1) | 360.2(1) | 120(1) |
| AS10 | 5.664(1) | 11.237(2) | 360.5(1) | 80(1) |
| AS15 | 5.650(1) | 11.298(2) | 360.6(1) | 100(1) |
| Not treated | 5.668(2) | 11.225(5) | 360.6(2) | 82(1) |
| Reference card | 5.642 | 11.25 | 358.11 | -— |



1099159x, 0, Downloaded from https://onlinelibrary.wiley.com/doi/10.1002/pip.70034 by Universita Milano Bicocca, Wiley Online Library on [25/11/2025]. See the Terms and Conditions (https://onlinelibrary.wiley.com/terms-and-conditions) on Wiley Online Library for rules of use; OA articles are governed by the applicable Creative Commons License

As for the CZTSSe compound, several S/Se solid solutions have been investigated in the literature in this space group [4]. All the investigated compositions obeyed Vegard's law, as depicted in Figure 8.

The AS (after selenization) samples exhibit a cell volume comparable to the not-treated one (not exposed to Cd(II) ions), suggesting a lack of incorporation of Cd(II) in the lattice of the AS CZTSSe compounds. In agreement with Vegard's law, the cell volume of 360.5 Å$^3$ for the not treated samples corresponds to a $Cu_2ZnSn(S_{0.15}Se_{0.85})_4$ composition (S/Se wt = 0.07). This result seems to be in agreement with the EDX experiments: the S/Se ratio is 0.06 in the not-treated reference samples, ranges from 0.06 to 0.09 for the AS samples, and falls within the 0.08–0.11 range for the BS samples.

The cell volumes of BS samples are slightly increased compared with the AS ones (up to 2 Å$^3$). This can be explained by assuming Cd(II) incorporation in the crystal lattice of CZTSSe, substituting for Zn(II), as confirmed by the EDX analysis: the BS samples contain 0.5–1 wt% of Cd.

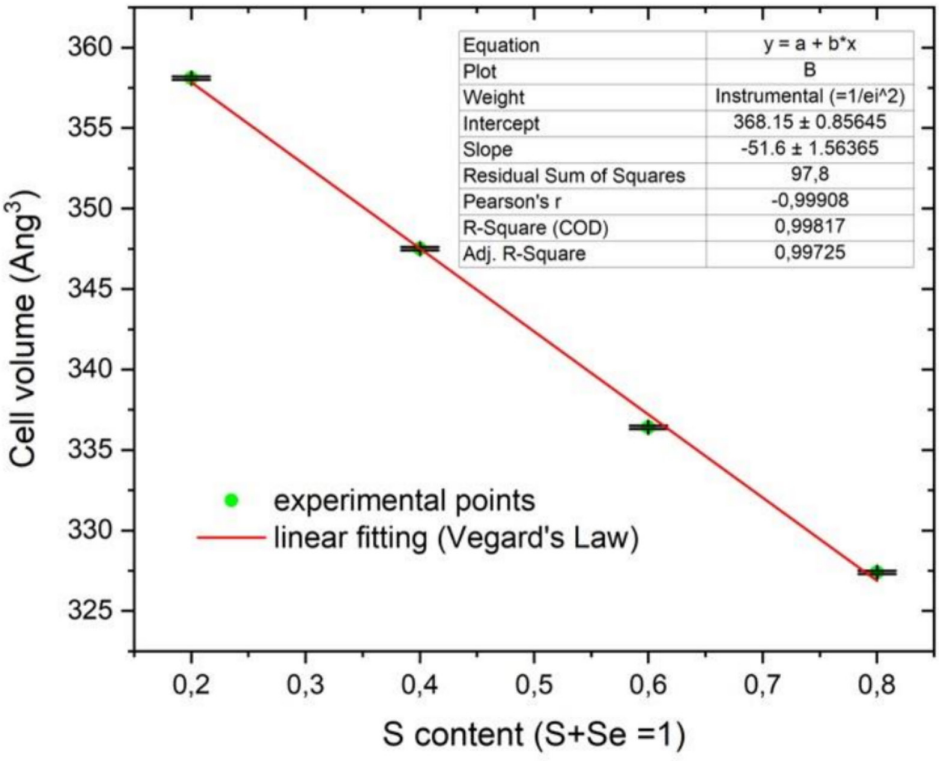


**FIGURE 8** | Relationship between cell volume and S content in the tetragonal CZTSSe samples.

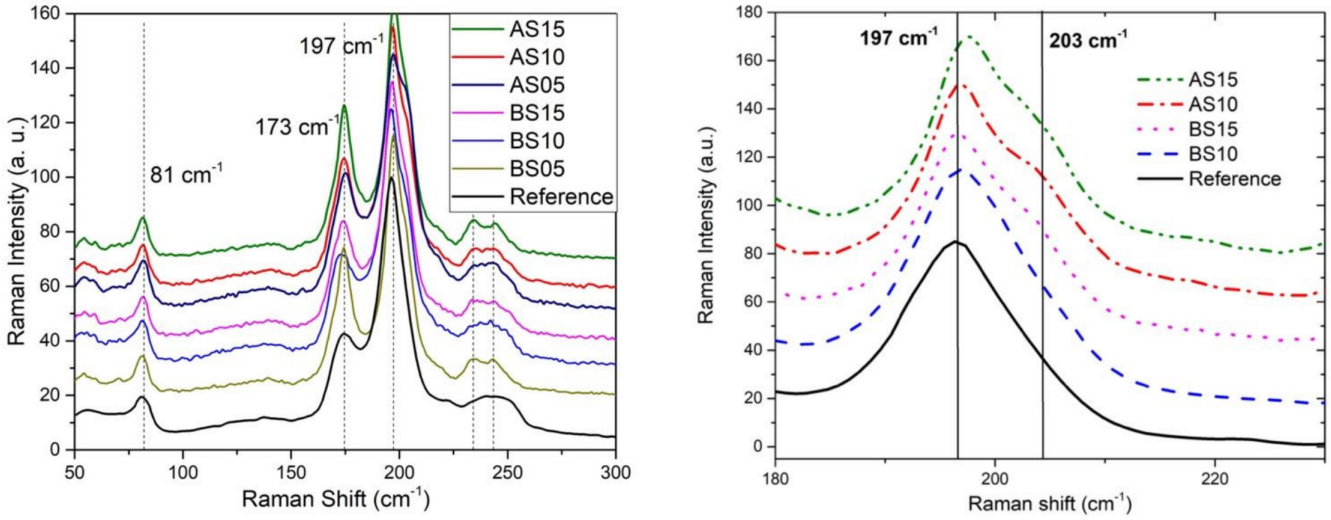


**FIGURE 9** | Raman spectra of the CZTSSe with excitation laser at 532 nm: reference (not treated absorber) compared with treated absorbers (with 5, 10, and 15 drops—05, 10, 15) before (BS) and after (AS) selenization (left); and detail of the 197 cm$^{-1}$ peak for not-treated, AS and BS absorbers in comparison (right).



1099159x, 0, Downloaded from https://onlinelibrary.wiley.com/doi/10.1002/pip.70034 by Universita Milano Bicocca, Wiley Online Library on [25/11/2025]. See the Terms and Conditions (https://onlinelibrary.wiley.com/terms-and-conditions) on Wiley Online Library for rules of use; OA articles are governed by the applicable Creative Commons License

### 3.2.3 | Raman Analysis

It is well known that, especially for kesterite, many possible secondary phases are not identifiable by X-ray diffraction patterns, and to have a careful analysis, an additional structural characterization with Raman spectroscopy is favorable. Raman spectra of the different cases are shown in Figure 9 (left). Also, in this case, we can observe the typical Raman peaks of the kesterite structure for all cases, and no particular peaks are attributed to secondary phases [3].

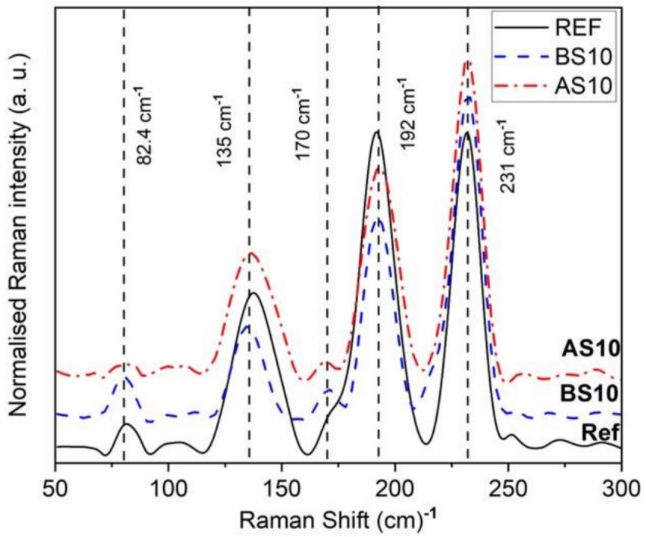


**FIGURE 10** | Raman spectra of the CZTSSe with excitation laser at 408 nm: reference (not treated absorber) compared with treated absorbers (with 10 drops) before (BS) and after (AS) selenization.

When we carefully analyze the main vibration (see Figure 9, right) at 197 $cm^{-1}$, no shift towards lower wavenumbers is observed for the BS-treated case compared with the not-treated one as expected from $Cu_2Zn_{1-x}Cd_xSn(S,Se)_4$ alloys [20]. A slight shift towards higher wavenumbers is instead observed for the AS-treated case, maybe due to an additional strain. However, in this case, the peak shows a large shoulder at 203 $cm^{-1}$, which can be attributed to CdSe [27, 28], and it could also be responsible for the slight shift of the CZTSSe prominent peak. Even at 150°C (temperature that follows the $CdCl_2$ deposition after selenization), selenium in excess reacts with cadmium deposited, forming CdSe particularly, but not only, at the grain boundaries. This CdSe peak in the Raman analysis is not visible in the XRD patterns, showing that this minimum amount of secondary phase is present on the surface, where selenium in excess is more likely to be found.

We have processed Raman analysis with a laser wavelength of 408 nm on BS10, AS10 and reference samples to compare with the 532-nm spectra and check for possible secondary phases (see Figure 10). The peaks identified with 532 nm are also confirmed in the 408 nm case; other peaks are also attributable to CZTSSe structure [3].

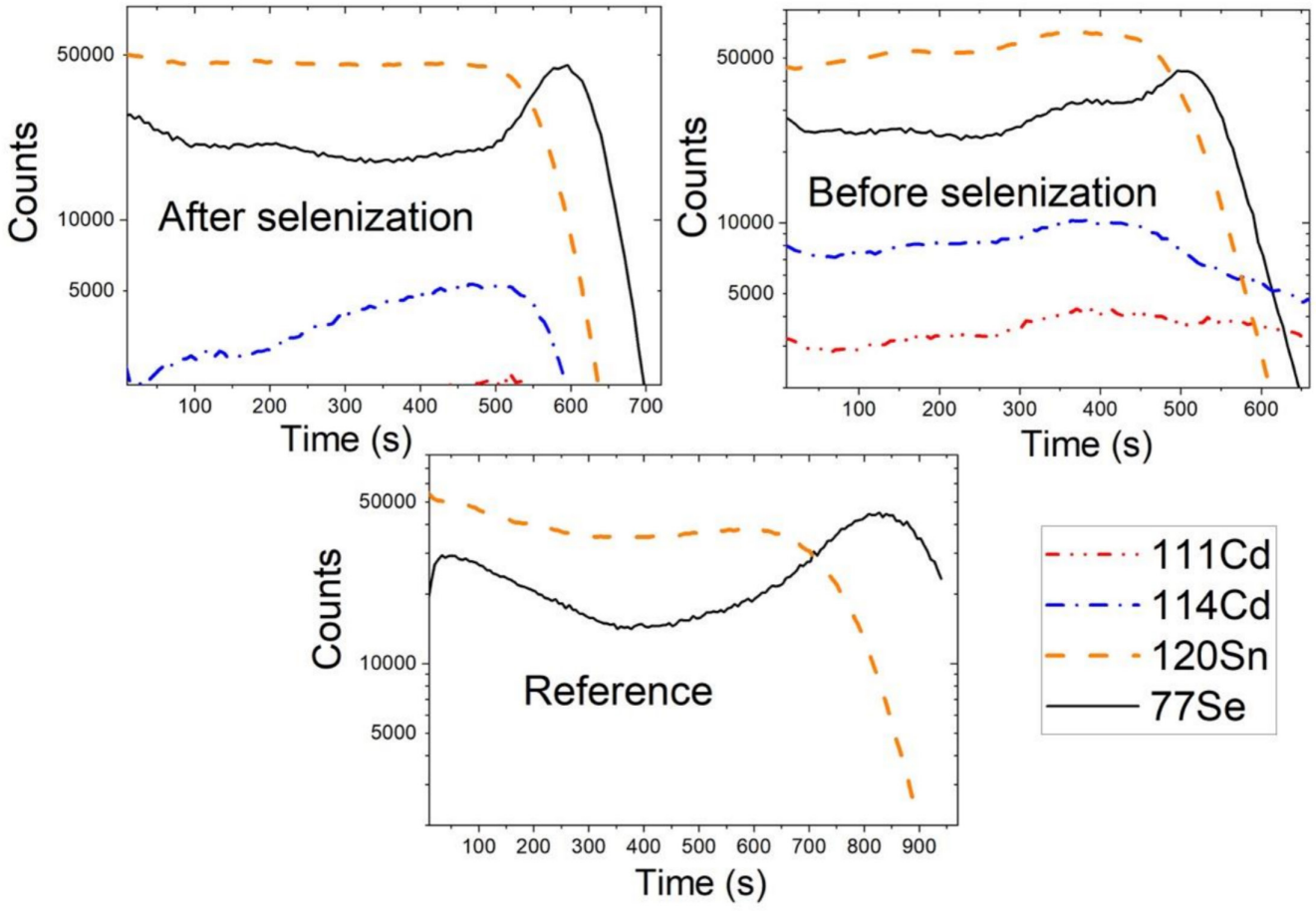


**FIGURE 11** | SIMS of CZTSSe treated after selenization (left), before selenization (right), not treated (below). The time represents the sputtering depth of the absorber: initial time → interface, maximum time → back contact.



1099159x, 0, Downloaded from https://onlinelibrary.wiley.com/doi/10.1002/pip.70034 by Universita Milano Bicocca, Wiley Online Library on [25/11/2025]. See the Terms and Conditions (https://onlinelibrary.wiley.com/terms-and-conditions) on Wiley Online Library for rules of use; OA articles are governed by the applicable Creative Commons License

So far, the presence and distribution of cadmium near the interface have been studied and described; however, it is essential to detect and analyze the effect of cadmium and its distribution in the bulk of the absorber from the interface down to the back contact.

### 3.2.4 | SIMS Analysis

In Figure 11, SIMS profiles of not treated, treated before selenization, and treated after selenization (both with 10 drops, viz., BS10 and AS10) absorbers are depicted. Selenium and tin were taken as a reference in all three cases, being the only two signals detectable for the not-treated case (a very low level for cadmium is observed, which is easily attributable to base noise). Cadmium, which was analyzed in its two main isotopes, $Cd^{111}$ and $Cd^{114}$, is observed in both treated cases but with a very different distribution. When $CdCl_2$ is applied before selenization, cadmium is evenly distributed across the whole absorber, with a slight reduction at the back contact; instead, when $CdCl_2$ is applied after selenization, the cadmium concentration tends to increase towards the back contact and suddenly drops.

Moreover, the concentration is rather different: In the AS case, we can observe only the most common isotope above the noise threshold, with almost half of the counts compared with the BS case. This instead shows signals for both isotopes well above the noise threshold.

So, we have another confirmation of the presence of cadmium in both treatment cases through the CZTSSe film. In both cases, the cadmium penetrates towards the back contact, but not in the same way. In the BS case, Cd diffusion into the bulk is driven by a much higher temperature (450°C of the selenization step) and happens during the phase formation of the absorber, resulting in a larger cadmium inclusion. On the other hand, the lower annealing temperature (150°C), that Cd undergoes in the AS case leads to a more negligible diffusion into the bulk, and it clearly cannot take part in the formation of the CZTSSe phase, done in the previous process step. This is also consistent with EDX results, which show Cd concentration only at the grain boundaries for AS while suggesting its incorporation into the matrix for the BS case. In the introduction, we have briefly discussed the possibility that Cd incorporation would affect the S/Se grading through the absorber; however, the Se signal for all three cases shows a similar behavior: slightly higher near the interface, constant across the absorber and then increases at the interface with Mo.

## 3.3 | Improvements in the Device Properties

We have already observed the beneficial effects of the $CdCl_2$ treatment by measuring the conversion efficiency, pointing out the increase in current density for both cases and in open circuit voltage for the AS case. But how does the elemental cadmium affect the electrical properties of the absorber?

### 3.3.1 | EQE Analysis

External quantum efficiency analysis is reported in Figure 12; here, we present again the comparison of the cells that have not been treated, treated before selenization, and treated after selenization (both with 10 drops of $CdCl_2$).

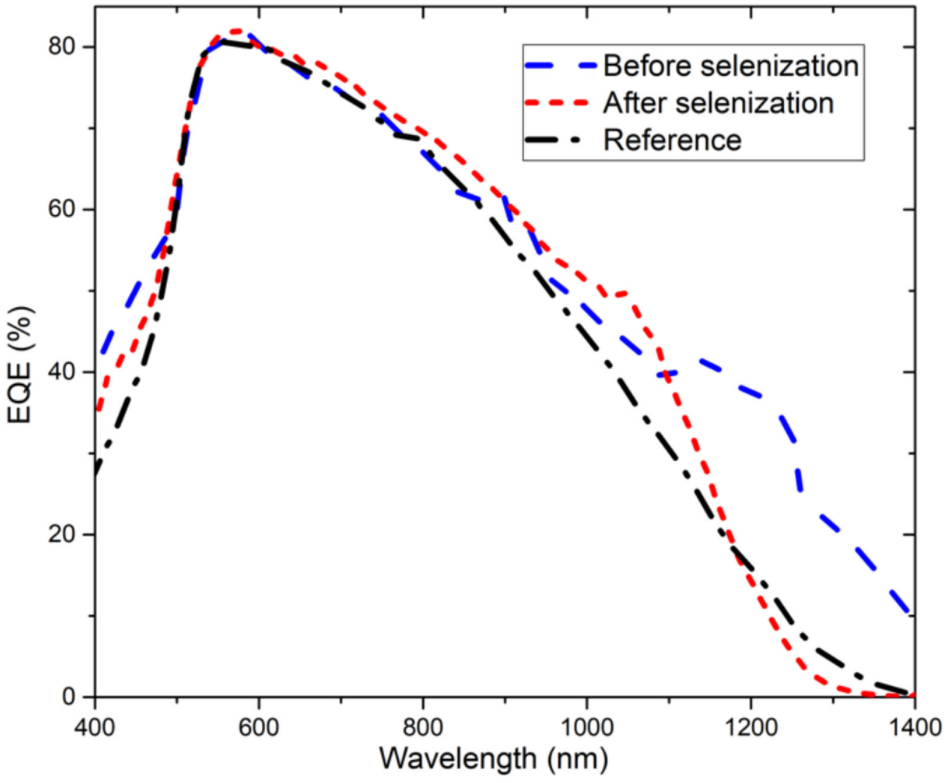


**FIGURE 12** | EQE spectra of CZTSSe-based devices with (1) not treated absorber, (2) treated before selenization, and (3) treated after selenization.



1099159x, 0, Downloaded from https://onlinelibrary.wiley.com/doi/10.1002/pip.70034 by Universita Milano Bicocca, Wiley Online Library on [25/11/2025]. See the Terms and Conditions (https://onlinelibrary.wiley.com/terms-and-conditions) on Wiley Online Library for rules of use; OA articles are governed by the applicable Creative Commons License

In the AS case, a higher response is observed at a longer wavelength, between 700 and 1100 nm, which is in accordance with the higher current density: the longer the wavelength, the larger the difference with the not-treated case. It appears that with cadmium included at the grain boundaries, as now attested by the structural characterization reported above, more carriers are collected far away from the interface, suggesting a possible passivation of recombination centers. These will be concentrated at the grain boundaries, coherently with what has been reported.

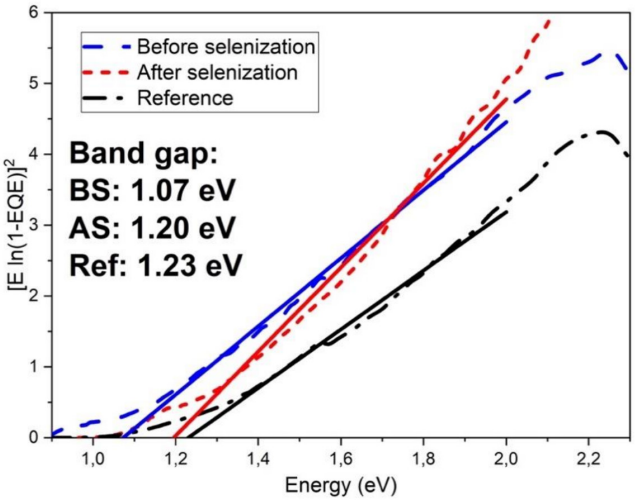


**FIGURE 13** | Extraction of the bandgaps from EQE analysis, using Tauc-plot method.

In the before-selenization treated case, we observe a higher response at longer wavelengths, extending into regions where the typical CZTSSe is off, given the typical band gap is around 1.2 eV (also considering the average S to Se ratio in these samples). The EQE response extends well beyond the 1400-nm range, suggesting that we are dealing with a transformed absorber that has a lower bandgap than the treated one.

To extract the band gap from the EQE curve, the wavelength ($\lambda$) is converted into photon energy (E), and $E*\ln(1-EQE)^2$ is plotted as a function of E; the band gap is extracted as the intercept with the energy axis [29]. The results are shown in Figure 13 and confirm an effective alloying of CZTSSe with cadmium and consequent reduction of the band gap, in accordance with what was observed by Xiao et al. [20]

However, in both $CdCl_2$ treated cases, we can observe a higher response with a respective increase in carrier collection. This effect needs to be confirmed, and how this relates to the presence of cadmium in the lattice and/or at the grain boundaries needs to be addressed.

### 3.3.2 | CV-DLCP Analysis

We have applied capacitance–voltage and drive-level capacitance profiling on the three cases reported in the paragraph above. The DLCP curves show consistently higher values compared with the CV ones. This contradicts the fact that CV is influenced by both shallow and deep defects, while DLCP is primarily affected by shallow defects [30]. However, this has

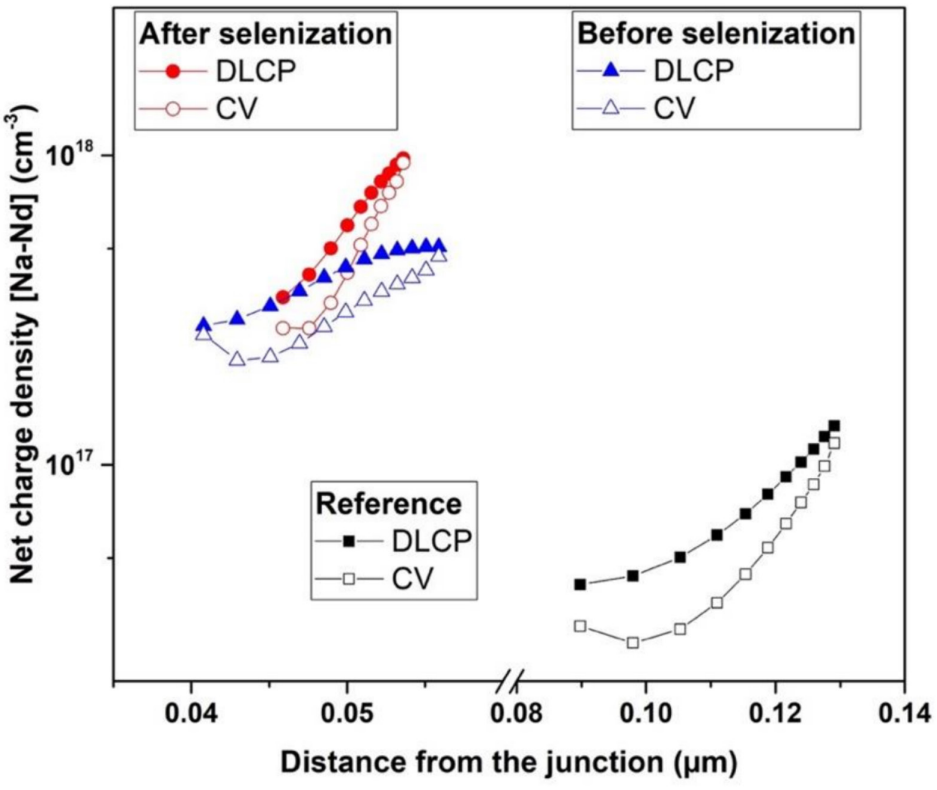


**FIGURE 14** | Capacitance–voltage (open dots) and drive level capacitance profiling (full dots) curves of CZTSSe-based devices with (1) not treated absorber (black); (2) treated before selenization (blue); (3) treated after selenization (red).



1099159x, 0, Downloaded from https://onlinelibrary.wiley.com/doi/10.1002/pip.70034 by Universita Milano Bicocca, Wiley Online Library on [25/11/2025]. See the Terms and Conditions (https://onlinelibrary.wiley.com/terms-and-conditions) on Wiley Online Library for rules of use; OA articles are governed by the applicable Creative Commons License

been observed in our samples also previously [14], and it can be explained by the presence of compensating deep donor defects that reduce the overall number of effective defects in the capacitance–voltage analysis.

However, when we compare the treated and not-treated finished devices (see Figure 14), there is a clear improvement in the carrier density when the $CdCl_2$ treatment is applied: the net charge density increases by one order of magnitude for both treated cases. So, whether cadmium is alloyed in the matrix lattice or included in the grain boundaries, it always results in effective absorber doping.

Moreover, by comparing the CV and DLCP curves, we can identify the number of compensating defects for each case. These results are primarily present in the reference case, without treatment, as observed in previous works [14]. Instead, the difference between DLCP and CV curves, in Figure 14, is more significant for the BS compared with the AS case, where the difference is, in some cases, extremely small. This suggests again that the cadmium, when located at the grain boundaries (as observed from the EDX analysis, see Figure 6), passivates them, reducing the compensating defects. These results confirm the doping effect of the cadmium deposited after selenization, while for the BS case, we have a slightly lower carrier concentration and a slightly higher amount of compensating defects compared with the AS case.

### 3.4 | Stability of the Cells

Stability of the solar cells is a very important value for the application of these devices in the real world. If a large area module cannot assure at least 80% of the initial efficiency within 25 years, it cannot be introduced in the market.

However, at this stage of the development, analysis of the stability is rather more important for addressing the diffusion of the inserted cadmium in order to understand if this element is included in the compound stoichiometry and when, instead, this does not happen anymore.

We have analyzed the initial stability of a large number of cells, corresponding to the different treatments, in a special accelerated stability test (AST) system where we heat the

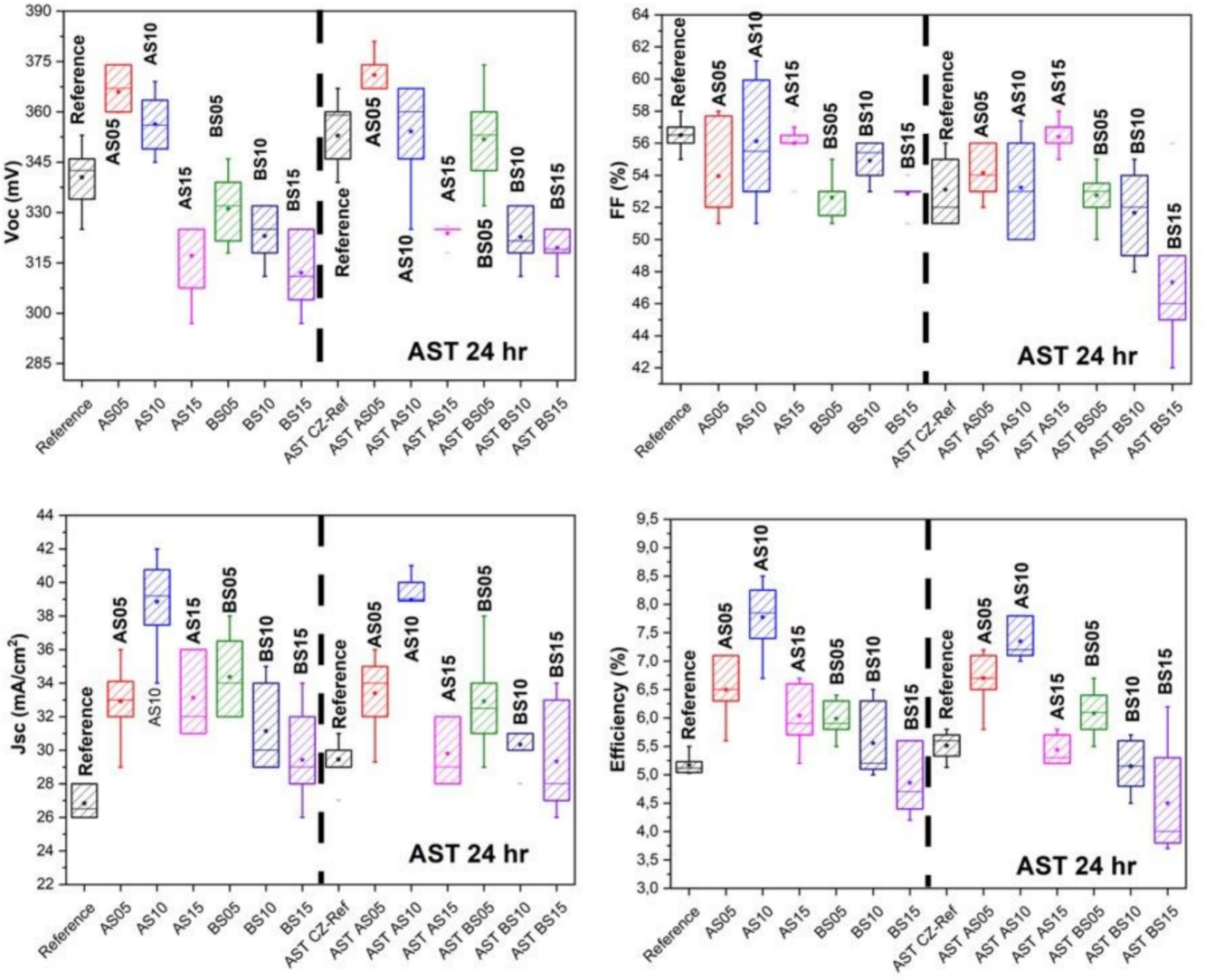


**FIGURE 15** | Comparison of statistical values of $J_{sc}$, $V_{oc}$, *FF*, and efficiency values before and after 24 h under 80°C and one sun illumination (AST 24 h).



1099159x, 0, Downloaded from https://onlinelibrary.wiley.com/doi/10.1002/pip.70034 by Universita Milano Bicocca, Wiley Online Library on [25/11/2025]. See the Terms and Conditions (https://onlinelibrary.wiley.com/terms-and-conditions) on Wiley Online Library for rules of use; OA articles are governed by the applicable Creative Commons License

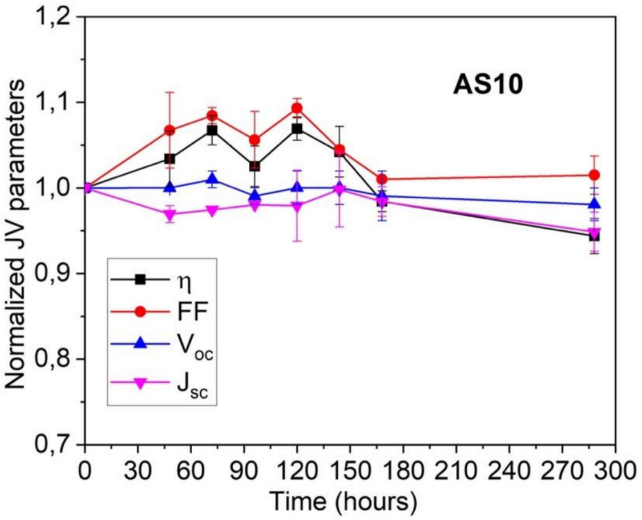


**FIGURE 16** | Average efficiency parameters, normalized to their initial values, of AS10 cells at different time steps of AST.

not-encapsulated devices at 80°C under one sun illumination, in order to have a reliable statistic. In Figure 15, the comparison of $V_{oc}$, $J_{sc}$, *FF*, and conversion efficiency before and after 24 h of accelerated aging is depicted. In general, the values do not change significantly. The values stay within the initial range demonstrating a good stability. $V_{oc}$ is generally very similar to the initial one, with a slight tendency to increase after AST, as the typical light soaking effect does. $J_{sc}$ is stable for all the samples. Instead, the fill factor has a reduction for the BS-case with 15 drops treatment. This might suggest that there is a certain threshold over which the cadmium goes in excess and cannot be included in the CZTSSe matrix, slightly diffusing through the junction, and resulting in a reduced fill-factor value.

Also, to have a more reliable confirmation of the stability of the $CdCl_2$-treated cells, a number of devices fabricated with the best efficiency configuration (AS10) have been aged for a much longer time, up to about 300 h that considering the multiplication factor of AST for 80°C and one sun, roughly corresponds to 1200 effective days of operation. Again, this was done on not-encapsulated devices. The result of this analysis is shown in Figure 16. After an initial *FF* increase, mostly attributable to light-soaking effects, the electrical parameters stay within the range of the initial values, confirming the high level of stability of these cells.

## 4 | Conclusions

We have introduced a new, simple and fast method for incorporating cadmium into CZTSSe devices. This method consists of dropping a $CdCl_2$ solution on the surface of the absorber and subsequently heating in air at 150°C. It is known that cadmium can either alloy or dope the absorber; our method, depending on the stage of the fabrication process in which it is introduced, can lead to Cd alloying or doping. In particular, if the treatment is performed before the final formation of the CZTSSe compound (before selenization), the result will be a $Cu_2Zn_{1-x}Cd_xSn(S,Se)_4$ alloy, while if it is carried out after selenization, we will obtain a Cd-doped CZTSSe. $CdCl_2$ processing is well known to be strongly beneficial for CdTe-based devices. In that case, a complete recrystallization of the layer occurs with a reorientation of the grains, enlargement of the grain size, and passivation at the grain boundaries. In the case of CZTSSe, a change in orientation and size of the grains is not observed, while a slight change in the morphology is registered for the BS case. Nevertheless, cadmium is included in the absorber: (1) in the matrix when the treatment is applied prior to the typical selenization step and (2) at the grain boundaries when the treatment is applied after selenization. The cadmium is diffused through the absorber down to the back contact, with higher concentration and homogeneously distributed for the BS case, slightly more concentrated in the proximity of the back contact in the AS case. The cadmium presence increases the overall performance of the solar cells, with a larger effect for the AS case due to the increase in the carrier concentration and the passivation of the grain boundaries, consequently reducing compensating defects. When the treatment is applied before selenization, an alloying of the absorber occurs with a reduction of the band gap, which results in higher current densities despite a slight recorded reduction of the open circuit voltage.

The application of cadmium on CZTSSe needs to be addressed also in terms of toxicity impact. The calculation on the amount of cadmium inserted from the methanol solution would be misleading because we wash away the cadmium chloride in excess, so we have considered the weight percentage given by EDX: 0.7% in weight (which stays constant according to the SIMS results; see Figure 11). With CZTSSe deposited on an area of $3\times3$ $cm^2$, with an absorber thickness of 1.6 μm (as described above) the volume of the absorber is $14.4*10^{-4}cm^3$. Considering that the density of CZTSSe can range from 4.5 to 5.6 $g\,cm^{-3}$ [31], we can calculate a quantity of material which is in the average of 0.0072 g. So, the calculated amount of Cd in the compound is $5*10^{-5}$ g. Considering a glass substrate of just 1 mm (the typical substrate used is 3 mm thick), and a typical glass density of 2.5 $g/cm^3$, we have on a $3\times3\,cm^2$ substrate a weight of 2.25 g. Calculating the percentage of 0.0072 g over a 2.25 g, we have a value of 0.002% (the actual value would be slightly lower if we consider the contribution of the whole solar cell stack).

One of the strictest directives in the world regarding the content of toxic elements in consumer products is the RoHS directive (Restriction of Hazardous Substances Directive) in the European Union (similar directives are extended to other countries). According to RoHS, the maximum permitted concentrations in nonexempt products are 0.1% or 1000 ppm for any toxic elements, except for cadmium, which is even more restricted to 0.01% or 100 ppm by weight. In this case, with a 1-mm glass (which is lower than usual) we are one order of magnitude lower than the most restricted Cd content, and with a 100-μm glass (flexible cells) we would still be within the RoHS range, attesting that the amount of cadmium used is even in this preliminary phase with no impact on the toxicity.

Depending on the desired application, this wet-$CdCl_2$ post-deposition treatment can be applied before or after the final formation of the CZTSSe, either alloying or doping the absorber, respectively, with a very simple and flexible process suitable for a wide variety of deposition techniques as a post-deposition treatment. This process has been patented under



1099159x, 0, Downloaded from https://onlinelibrary.wiley.com/doi/10.1002/pip.70034 by Universita Milano Bicocca, Wiley Online Library on [25/11/2025]. See the Terms and Conditions (https://onlinelibrary.wiley.com/terms-and-conditions) on Wiley Online Library for rules of use; OA articles are governed by the applicable Creative Commons License

the title "METHOD TO ENHANCE THE KESTERITE SOLAR CELL PERFORMANCE" (European patent: EP 4120367A1, US patent: 20230060927).

### Author Contributions

**Prabeesh Punathil:** review and editing, investigation, validation, visualization. **Elisa Artegiani:** review and editing, investigation, validation, visualization. **Solidea Zanetti:** investigation, visualization. **Simya O K:** investigation, validation, visualization. **Luca Lozzi:** investigation, formal analysis, visualization. **Andrea Gasparotto:** investigation, formal analysis, visualization. **Fabio Piccinelli:** investigation, formal analysis, visualization. **C. L. Boldrini:** investigation, visualization. **S. Binetti:** supervision, visualization, formal analysis. **Alessandro Romeo:** writing – original draft, review and editing, investigation, conceptualization, methodology, visualization, supervision, project administration, funding acquisition.


### Acknowledgments

This work was partially financed by project BISPRASOL (n. 1695-0015-1463-2019), Regione Veneto. This work has been partially funded by Fondazione Cariverona with the project INSOBILD Ref. 2022.0094, ID 52271, CUP B33C22001760007. The Technological Platform Center (CPT) at the University of Verona, in the person of Dr. Marco Giarola, is thankfully acknowledged for Raman measurements. Dott. Lorenzo Arrizza at the Microscopy Centre of the University of L'Aquila is thankfully acknowledged for the EDXS/SEM measurements. Open access publishing facilitated by Universita degli Studi di Verona, as part of the Wiley - CRUI-CARE agreement.

### Funding

This work was supported by Fondazione Cassa di Risparmio di Verona Vicenza Belluno e Ancona (52271) and Regione del Veneto (1695-0015-1463-2019).


### Conflicts of Interest

The authors declare no conflicts of interest.

### Data Availability Statement

The data that support the findings of this study are available from the corresponding author upon reasonable request.

### References


1. M. A. Green, E. D. Dunlop, M. Yoshita, et al., "Solar Cell Efficiency Tables (Version 64)," *Progress in Photovoltaics: Research and Applications* 32 (2024): 425–441, https://doi.org/10.1002/pip.3831.

2. C. Platzer Björkman, J. K. Larsen, N. Saini, M. Babucci, and N. Martin, "Ultrathin Wide Band Gap Kesterites," *Faraday Discussions* 239 (2022): 38–50, https://doi.org/10.1039/d2fd00052k.

3. M. Dimitrievska, F. Oliva, M. Guc, et al., "Defect Characterisation in $Cu_2ZnSnSe_4$ Kesterites: Via Resonance Raman Spectroscopy and the Impact on Optoelectronic Solar Cell Properties," *Journal of Materials Chemistry A* 7 (2019): 13293–13304, https://doi.org/10.1039/c9ta03625c.

4. F. Gao, S. Yamazoe, T. Maeda, K. Nakanishi, and T. Wada, "Structural and Optical Properties of In-Free $Cu_2ZnSn(S,Se)_4$ Solar Cell Materials," *Japanese Journal of Applied Physics* 51 (2012): 10NC29, https://doi.org/10.1143/JJAP.51.10NC29.

5. S. Ahn, S. Jung, J. Gwak, et al., "Determination of Band Gap Energy ($E_g$) of $Cu_2ZnSnSe_4$ Thin Films: On the Discrepancies of Reported Band Gap Values," *Applied Physics Letters* 97 (2010): 021905, https://doi.org/10.1063/1.3457172.

6. P. Prabeesh, P. Saritha, I. P. Selvam, and S. N. Potty, "Fabrication of CZTS Thin Films by Dip Coating Technique for Solar Cell Applications," *Materials Research Bulletin* 86 (2017): 295–301, https://doi.org/10.1016/j.materresbull.2016.10.033.

7. P. Prabeesh, V. G. Sajeesh, I. Packia Selvam, M. S. Divya Bharati, G. Mohan Rao, and S. N. Potty, "CZTS Solar Cell With Non-Toxic Buffer Layer: A Study on the Sulphurization Temperature and Absorber Layer Thickness," *Solar Energy* 207 (2020): 419–427, https://doi.org/10.1016/j.solener.2020.06.103.

8. G. Altamura, M. Wang, and K. Choy, "Improving Efficiency of Electrostatic Spray-Assisted Vapor Deposited $Cu_2ZnSn(S,Se)_4$ Solar Cells by Modification of Mo/Absorber Interface," *Thin Solid Films* 597 (2015): 19–24, https://doi.org/10.1016/j.tsf.2015.11.027.

9. P. M. P. Salome, F. M. Matinaga, and J. C. Gonza, "Growth and Characterization of $Cu_2ZnSn(S,Se)_4$ Thin Films for Solar Cells," *Solar Energy Materials and Solar Cells* 101 (2012): 147–153, https://doi.org/10.1016/j.solmat.2012.02.031.

10. J. Y. Park, R. B. V. Chalapathy, A. C. Lokhande, C. W. Hong, and J. H. Kim, "Fabrication of Earth Abundant $Cu_2ZnSnSSe_4$ (CZTSSe) Thin Film Solar Cells With Cadmium Free Zinc Sulfide (ZnS) Buffer Layers," *Journal of Alloys and Compounds* 4 (2016): 395, https://doi.org/10.1016/j.jallcom.2016.11.178.

11. C. M. Fella, A. R. Uhl, Y. E. Romanyuk, and A. N. Tiwari, "$Cu_2ZnSnSe_4$ Absorbers Processed From Solution Deposited Metal Salt Precursors Under Different Selenization Conditions," *Physica Status Solidi* 209 (2012): 1043–1048, https://doi.org/10.1002/pssa.201228003.

12. Y. E. Romanyuk, S. G. Haass, S. Giraldo, et al., "Doping and Alloying of Kesterites," *Journal of Physics: Energy* 1 (2019): 044004, https://doi.org/10.1088/2515-7655/ab23bc.

13. A. D. Collord and H. W. Hillhouse, "Germanium Alloyed Kesterite Solar Cells With Low Voltage Deficits," *Chemistry of Materials* 28 (2016): 2067–2073, https://doi.org/10.1021/acs.chemmater.5b04806.

14. P. Punathil, E. Artegiani, S. Zanetti, L. Lozzi, V. Kumar, and A. Romeo, "A Simple Method for Ge Incorporation to Enhance Performance of Low Temperature and Non-Vacuum Based CZTSSe Solar Cells," *Solar Energy* 236 (2022): 599–607, https://doi.org/10.1016/j.solener.2022.03.027.

15. O. K. Simya, I. Anefnaf, P. Punathil, et al., "Impact of Lithium as Interfacial Treatment for CZTSSe Solar Cells," in *Conference Record of the IEEE Photovoltaic Specialists Conference*, (Institute of Electrical and Electronics Engineers Inc, 2024), 640–644, https://doi.org/10.1109/PVSC57443.2024.10749209.

16. S. Kumar, D. K. Sharma, and S. Auluck, "Stability, Electronic, and Optical Properties of Wurtzite $Cu_2Cd_xZn_{1-x}SnS_4$ Alloys as Photovoltaic Materials: First-Principles Insight," *Physical Review B: Condensed Matter* 94 (2016): 235206, https://doi.org/10.1103/PhysRevB.94.235206.

17. J. Fu, Q. Tian, Z. Zhou, et al., "Improving the Performance of Solution-Processed $Cu_2ZnSn(S,Se)_4$ Photovoltaic Materials by $Cd^{2+}$ Substitution," *Chemistry of Materials* 28 (2016): 5821–5828, https://doi.org/10.1021/acs.chemmater.6b02111.

18. J. C. Slater, "Atomic Radii in Crystals," *Journal of Chemical Physics* 41 (1964): 3199–3204, https://doi.org/10.1063/1.1725697.

19. L. Grenet, M. A. A. Suzon, F. Emieux, and F. Roux, "Analysis of Failure Modes in Kesterite Solar Cells," *ACS Applied Energy Materials* 1 (2018): 2103–2113, https://doi.org/10.1021/acsaem.8b00194.

20. Z. Y. Xiao, Y. F. Li, B. Yao, et al., "Bandgap Engineering of $Cu_2Cd_xZn_{1-x}SnS_4$ Alloy for Photovoltaic Applications: A Complementary Experimental and First-Principles Study," *Journal of Applied Physics* 114 (2013): 183506, https://doi.org/10.1063/1.4829457.





1099159x, 0, Downloaded from https://onlinelibrary.wiley.com/doi/10.1002/pip.70034 by Universita Milano Bicocca, Wiley Online Library on [25/11/2025]. See the Terms and Conditions (https://onlinelibrary.wiley.com/terms-and-conditions) on Wiley Online Library for rules of use; OA articles are governed by the applicable Creative Commons License

21. J. Andrade-Arvizu, R. F. Rubio, V. Izquierdo-Roca, et al., "Controlling the Anionic Ratio and Gradient in Kesterite Technology," *ACS Applied Materials & Interfaces* 14 (2022): 1177–1186, https://doi.org/10.1021/acsami.1c21507.

22. J. Andrade-Arvizu, V. Izquierdo-Roca, I. Becerril-Romero, et al., "Is It Possible to Develop Complex S-Se Graded Band Gap Profiles in Kesterite-Based Solar Cells?," *ACS Applied Materials & Interfaces* 11 (2019): 32945–32956, https://doi.org/10.1021/acsami.9b09813.

23. P. Punathil, S. Zanetti, E. Artegiani, V. Kumar, and A. Romeo, "Analysis of the Drying Process for Precursors of $Cu_2ZnSn(S,Se)_4$ Layers by Low Cost Non Vacuum Fabrication Technique," *Solar Energy* 224 (2021): 992–999, https://doi.org/10.1016/j.solener.2021.06.063.

24. A. Romeo, S. Buecheler, M. Giarola, et al., "Study of CSS- and HVE-CdTe by Different Recrystallization Processes," *Thin Solid Films* 517 (2009): 2132–2135, https://doi.org/10.1016/j.tsf.2008.10.129.

25. B. E. McCandless, "Thermochemical and Kinetic Aspects of Cadmium Telluride Solar Cell Processing," in: Proceedings of the 2001 MRS Spring Meeting, p. H1.6, 1–12, 2001.

26. H. Luan, B. Yao, Y. Li, et al., "Mechanism of Enhanced Power Conversion Efficiency of $Cu_2ZnSn(S,Se)_4$ Solar Cell by Cadmium Surface Diffusion Doping," *Journal of Alloys and Compounds* 876 (2021): 160160, https://doi.org/10.1016/j.jallcom.2021.160160.

27. Y. Gao and P. G. Yin, "Synthesis of Cubic CdSe Nanocrystals and Their Spectral Properties," *Nanomaterials and Nanotechnology* 7 (2017): 1–6, https://doi.org/10.1177/1847980417701747.

28. Y. T. Nien, B. Zaman, J. Ouyang, I. G. Chen, C. S. Hwang, and K. Yu, "Raman Scattering for the Size of CdSe and CdS Nanocrystals and Comparison With Other Techniques," *Materials Letters* 62 (2008): 4522–4524, https://doi.org/10.1016/j.matlet.2008.08.023.

29. R. Carron, C. Andres, E. Avancini, et al., "Bandgap of Thin Film Solar Cell Absorbers: A Comparison of Various Determination Methods," *Thin Solid Films* 669 (2019): 482–486, https://doi.org/10.1016/j.tsf.2018.11.017.

30. J. T. Heath, J. D. Cohen, and W. N. Shafarman, "Bulk and Metastable Defects in $CuIn_{1-x}Ga_xSe_2$ Thin Films Using Drive-Level Capacitance Profiling," *Journal of Applied Physics* 95 (2004): 1000–1010, https://doi.org/10.1063/1.1633982.

31. L. Guen and W. S. Glaunsinger, "Electrical, Magnetic, and EPR Studies of the Quaternary Chalcogenides $Cu_2A^{II}B^{IV}X_4$ Prepared by Iodine Transport," *Journal of Solid State Chemistry* 35 (1980): 10–21, https://doi.org/10.1016/0022-4596(80)90457-0.



1099159x, 0, Downloaded from https://onlinelibrary.wiley.com/doi/10.1002/pip.70034 by Universita Milano Bicocca, Wiley Online Library on [25/11/2025]. See the Terms and Conditions (https://onlinelibrary.wiley.com/terms-and-conditions) on Wiley Online Library for rules of use; OA articles are governed by the applicable Creative Commons License